Pure phonon anharmonicity and the anomalous thermal expansion of silicon

D.S. Kim,[1,*] O. Hellman,[1] J. Herriman,[1] H.L. Smith,[1] J.Y.Y. Lin,[2] N. Shulumba,[3] J.L. Niedziela,[4] C.W. Li,[5] D.L. Abernathy,[6] and B. Fultz[1]

[1] *California Institute of Technology, Department of Applied Physics and Materials Science, Pasadena, California 91125, USA*
[2] *Neutron Data Analysis and Visualization Division, Oak Ridge National Laboratory, Oak Ridge, Tennessee 37831, USA*
[3] *California Institute of Technology, Department of Mechanical and Civil Engineering, Pasadena, California 91125, USA*
[4] *Instrument and Source Division, Oak Ridge National Laboratory, Oak Ridge, Tennessee 37831, USA*
[5] *University of California Riverside, Department of Mechanical Engineering, Riverside, California 92521, USA*
[6] *Quantum Condensed Matter Division, Oak Ridge National Laboratory, Oak Ridge, Tennessee 37831, USA*

(Dated: October 28, 2016)

Despite the widespread use of silicon in modern technology, its peculiar thermal expansion is not well-understood. Harmonic phonons adapted to the specific volume at temperature, quasiharmonic approximation, has become accepted for simulating the thermal expansion, but has given ambiguous interpretations for microscopic mechanisms. To test the atomistic mechanisms, we performed inelastic neutron scattering experiments on a single crystal of silicon to measure the changes in lattice dynamics from 100 to 1500 K. Our state-of-the-art ab initio calculations, which fully account for phonon anharmonicity, reproduced the measured shifts of individual phonons with temperature, whereas the quasiharmonic approximation typically gave results of the wrong sign. Surprisingly, the accepted quasiharmonic model was found to predict the thermal expansion owing to a fortuitous cancellation of contributions from individual phonons.

A quantized harmonic oscillator was Einstein's seminal idea for understanding atom vibrations in solids. Better accuracy for crystalline solids is achieved when the vibrations are resolved into normal modes. Each normal mode is quantized, with excitations called phonons. However, harmonic models are limited to quadratic terms in the interatomic potential, and it is well-known that higher order terms in the interatomic potential are necessary to describe properties of real solids such as thermal conductivity and thermal expansivity. Despite this knowledge, the best way to account for non-harmonic effects remains less clear. A popular approach is the quasiharmonic model (QH), which assumes harmonic oscillators, but with frequencies renormalized to account for the thermal expansion. In a quasiharmonic model, the energy of the phonon mode i changes with crystal volume, V. Changes to phonon energies are usually described by a mode Grüneisen parameter, $\gamma_i = -\frac{V}{\varepsilon_i}\frac{\partial \varepsilon_i}{\partial V}$, where $\varepsilon_i = \hbar\omega_i$ is the mode energy (and $\omega_i/2\pi$ is the mode frequency). A positive γ gives a reduction in mode energy with thermal expansion increasing the vibrational entropy ΔS_{vib}. At finite temperature, the extra elastic energy from thermal expansion, ΔE_{el}, is offset by the term $-T\Delta S_{\text{vib}}$ in the free energy $\Delta F = \Delta E_{\text{el}} - T\Delta S_{\text{vib}}$ [1, 2]. For positive γ, this free energy is minimized with a positive thermal expansion, so for negative γ, a negative thermal expansion is expected.

The cubic and quartic terms of the interatomic potential cause the normal modes to interact and exchange energy. This is pure anharmonicity, where the the energy of a phonon is altered by the presence of other phonons at finite temperatures, irrespective of the volume of the solid. Anharmonic effects increase with larger thermal atomic displacements. Sometimes this causes a misperception that pure anharmonicity is important only at high temperatures, and quasiharmonic models may be valid at low and moderate temperatures owing to low phonon populations. However, the leading-order terms of both quasiharmonicity and anharmonicity are linear in temperature [3], so if anharmonicity is important at high temperatures, it can have the same relative importance at low temperatures, too.

Finding the relative importances of quasiharmonicity and anharmonicity should be done by quantitative analysis, but to date the dominance of quasiharmonicity for silicon has been assumed in part because quasiharmonic models predict the thermal expansion with reasonable accuracy [4–6]. The quasiharmonic model predicts the anomalous negative thermal expansion of silicon from 10 K to 125 K and the low thermal expansion up to the melting temperature [7–11]. The positive thermal expansion coefficients observed at moderate and high temperatures are anomalous in their own right – they are small compared to diamond and other materials with zinc-blende structures [9]. Further validation of the quasiharmonic approximation was provided by measurements of the Raman mode and a few second-order Raman modes of silicon under pressure, which was accurately predicted by volume-dependent density functional theory (DFT) calculations at low temperature [12, 13]. The negative Grüneisen parameters of the low-energy transverse acoustic (TA) modes have received considerable attention and have been attributed to the "open-ness" of the diamond cubic structure [11], the stability of angular forces [6], or entropy in general [5].

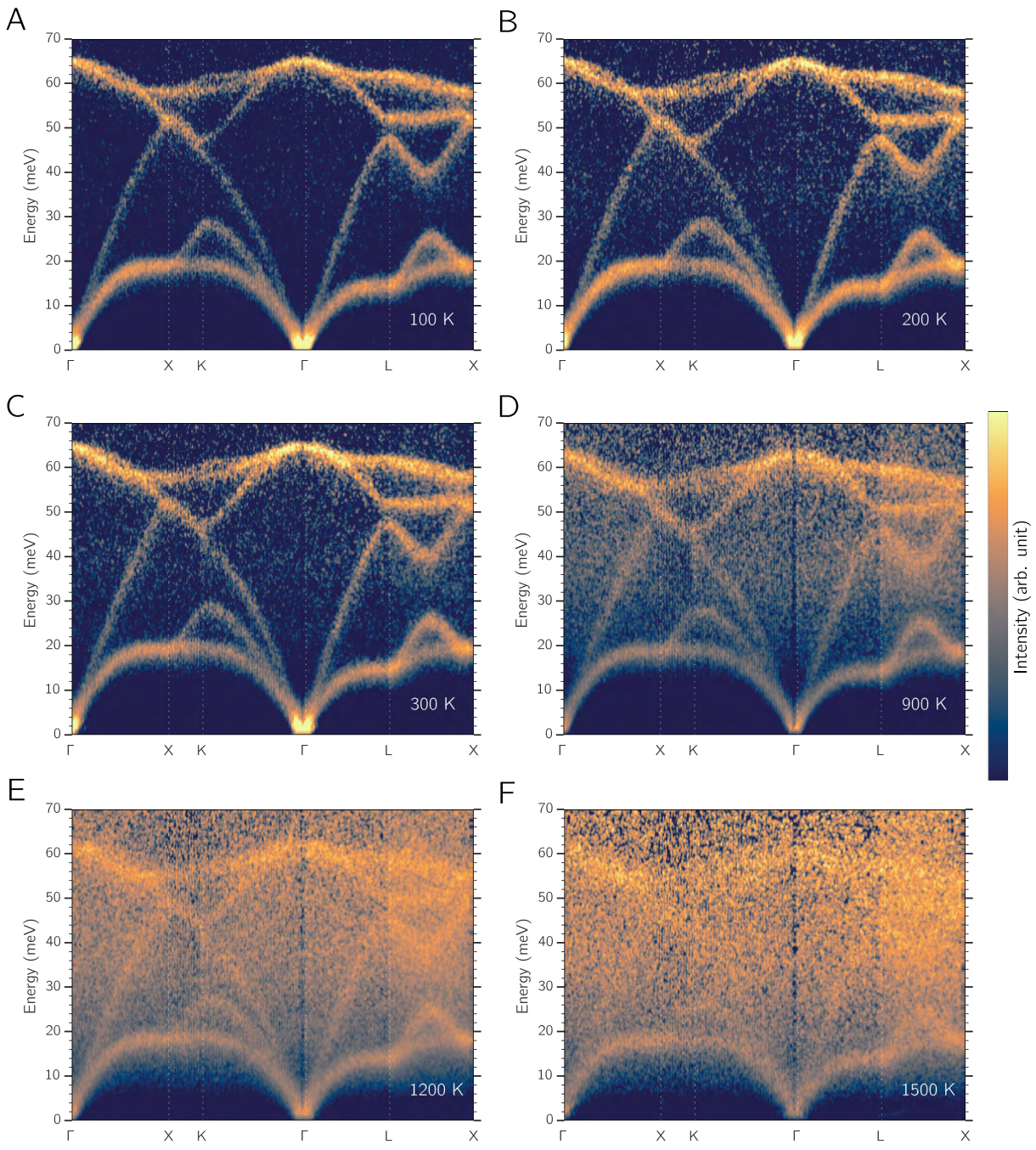

FIG. 1. **Experimental phonon dispersions of silicon.** Reduced and 'folded' inelastic neutron scattering data of silicon measured at (**A**) 100 K, (**B**) 200 K, (**C**) 300 K, (**D**) 900 K, (**E**) 1200 K, (**F**) 1500 K.

Nevertheless, the precise role of the TA modes in thermal expansion remains unclear [4, 6]. With increasing temperature, phonons are excited in higher-energy phonon branches, and their positive Grüneisen parameters are expected to cause the overall thermal expansion to change sign (as discussed in the Supplementary Materials).

"Non-trivial" phonon shifts that were not accounted for by thermal expansion were reported in an earlier experimental paper on phonon dispersions in silicon up to 300 K [14]. The importance of pure anharmonicity in temperature-dependent phonon shifts at moderate and high temperatures was also found in work based on molecular dynamics, many-body perturbation theory, and *ab initio* calculations on silicon [15–21]. (Nuclear quantum effects were shown to be important, but nuclear quantum effects alone do not reproduce the correct thermal expansion coefficients

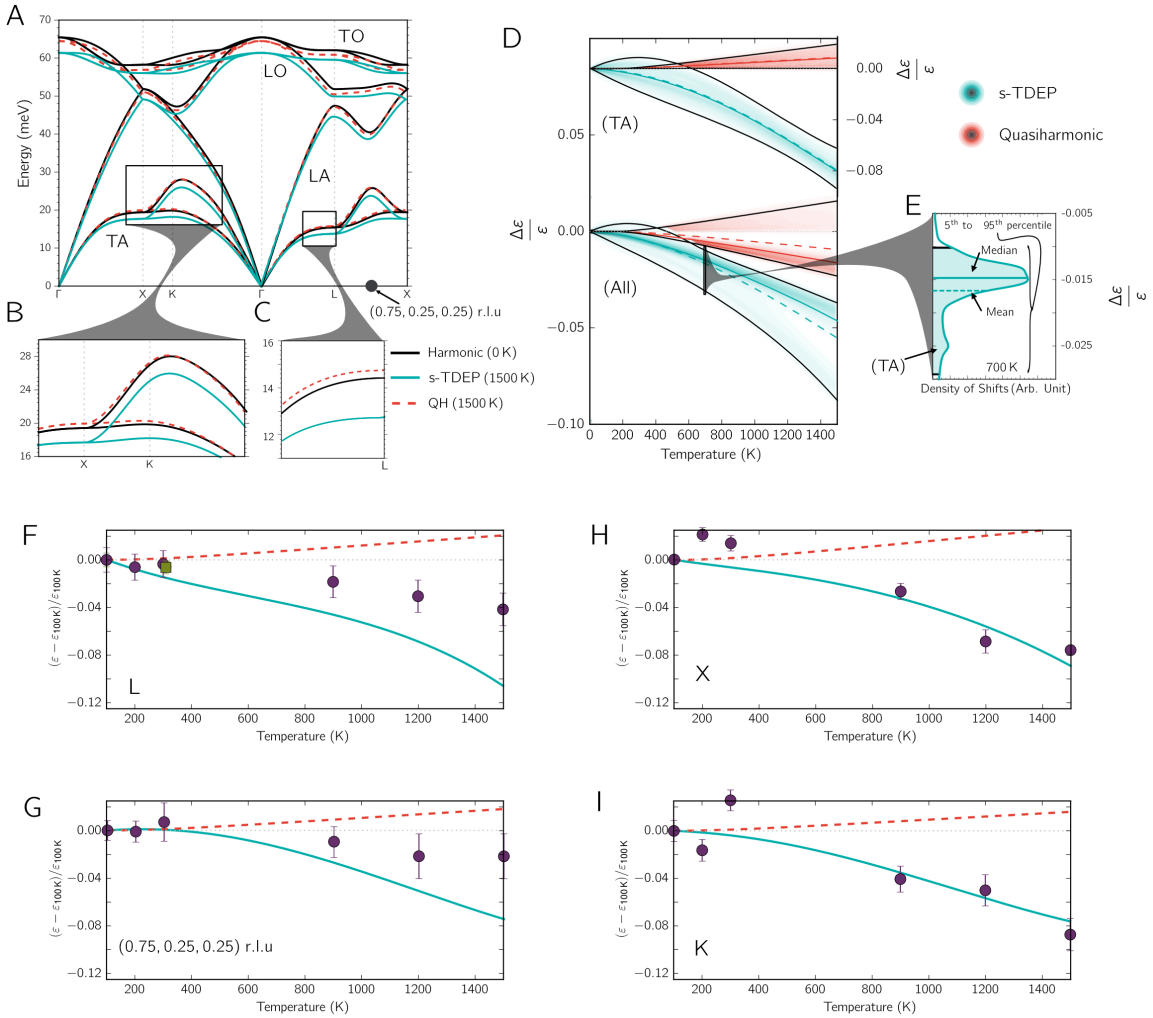

FIG. 2. **A comparison between s-TDEP and quasiharmonic *ab initio* calculations throughout the Brillouin zone. A-C**, Phonon dispersions of silicon from *ab initio* density functional theory calculations at 0 K (black solid line), and 1500 K in the quasiharmonic approximation (red dashed line) and s-TDEP (teal solid line) with transverse acoustic (TA), longitudinal acoustics (LA), longitudinal optical (LO), transverse optical (TO) branches labeled. The (0.75,0.25,0.25)-point is shown as a black circle marker for reference. Inset shows transverse acoustic modes along paths from around Γ-X-K (**B**), and a small portion of Γ-L (**C**). **D**, Density of fractional phonon energy shifts with temperature. The densities from all branches (s-TDEP: teal, quasiharmonic (QH): red) and densities from just the low transverse modes are offset and scaled for clarity. Contour of densities are in color intensity, and the mean (dashed color line) and median (solid color lines) for each distribution are also shown with the 5^{th} to 95^{th} percentile shown as solid black lines. **E**, The density of the 700 K s-TDEP is shown. Notice the more negative peak consists of a majority of TA-modes.

[22, 23].) Temperature-dependent phonon shifts from pure phonon anharmonicity should alter significantly the predictions of thermal expansion based on negative Grüneisen parameters and the quasiharmonic approximation. A more detailed study of phonons in silicon at high temperatures is therefore appropriate because very few modes were previously assessed [14, 20].

The phonon dispersions of silicon had never been measured at temperatures above 300 K, and we undertook the experiments to do so on a high-purity single crystal of silicon (mass ≈ 28.5 g) with ⟨110⟩-orientation, machined into a tube for optimal neutron scattering properties. The sample was rotated in a furnace on a direct geometry time-of-flight inelastic neutron scattering spectrometer (ARCS) [24] at the Spallation Neutron Source at Oak Ridge National Laboratory. The data were reduced to give all phonon dispersions in the irreducible wedge of the first Brillouin zone. Our "folding" technique of summing all of the $S(\mathbf{q}, \varepsilon)$ data (from >100 Brillouin zones) into an irreducible wedge increases the signal strength, suppresses polarization effects that alter intensities in some Brillouin zones [25], and averages out any possible effects of "an-

harmonic interference" [26].

Fig. 1 shows phonon dispersions as bright intensities. The dispersions at low temperatures are in excellent agreement with previous work that used triple-axis spectrometers [14, 27]. The smooth background between the phonon dispersions is dominated by multiphonon scattering [28]. With increasing temperature, the majority of phonon modes, including the low-energy transverse acoustic modes, soften in proportion to their energy, i.e., the mode Grüneisen parameters are similar. This self-similar behavior of phonon softening was reported previously [21].

All *ab initio* calculations were performed with the VASP package. A stochastically-initialized temperature-dependent effective potential method (s-TDEP) [12, 29, 30] was implemented to obtain phonon shifts with temperature, including intrinsic phonon anharmonicities and nuclear quantum effects. Quasiharmonic calculations were also conducted as described previously [21]. Methods for both the measurements and the calculations are described in the Supplementary Materials.

Results from calculations by the s-TDEP method (with anharmonicity and thermal expansion) and conventional quasiharmonic *ab initio* calculations (with no anharmonicity) are shown in Fig. 2. There are large discrepancies in the signs and magnitudes of phonon energy shifts between the two models. Most interestingly, Fig. 2.**B,C** show that the s-TDEP calculations predict a reduction in phonon energy, "softening", in the transverse modes (roughly < 35 meV), whereas the quasiharmonic calculations predict an increase in phonon energy, "stiffening", at 1500 K (with negative Grüneisen parameters as reported previously [4–6]).

We calculated the fractional shifts of energies for all phonon modes in the first Brillouin zone, $\Delta\varepsilon/\varepsilon\,(T)$. The phonon modes ($\varepsilon_i$) were calculated using a 50×50×50 grid of **q**-points. Fig. 2.**D** compares the density of fractional phonon shifts from quasiharmonic and anharmonic (s-TDEP) calculations. The density of fractional shift, $\rho\,(\Delta\varepsilon/\varepsilon)$, is shown in Fig. 2.**E** from the s-TDEP method at 700 K. Compared to the quasiharmonic predictions for the TA modes (shown at top of Fig. 2.**D**), the anharmonic shifts are an order-of-magnitude larger, have opposite signs, and follow opposite thermal trends. Such large discrepancies allow for definitive experimental tests.

Individual phonon energies were obtained from constant-**q** fits to the measured $S(\mathbf{q}, \varepsilon)$, as shown in the Supplementary Materials. Fig. 2.**F-I** show that the trends from the anharmonic s-TDEP calculations are in far better agreement with experiment than the quasiharmonic trends. Thermal trends for phonons at the L,X,K-points (Fig. 2.**F-H**) are presented for their importance in the interpretation of quasiharmonic results [4]. Another example for a phonon mode located away from a high-symmetry line is shown in Fig.2.**I**.

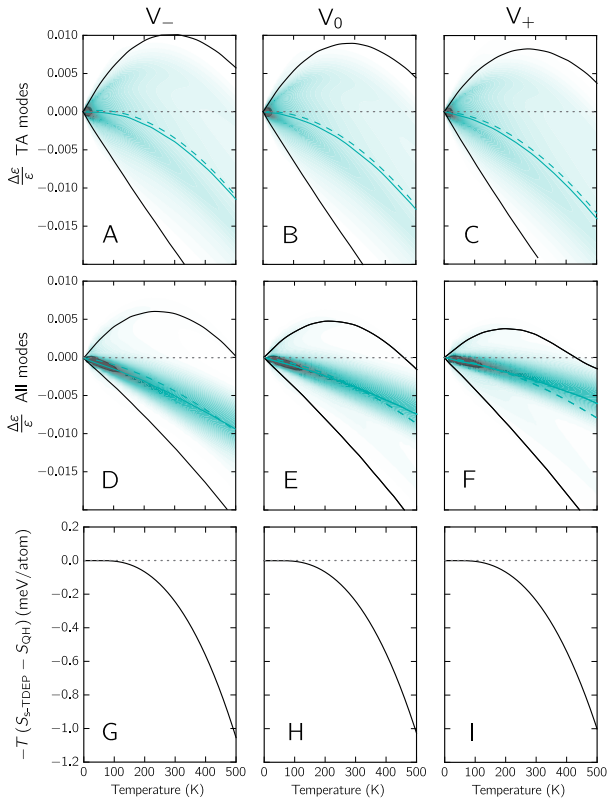

FIG. 3. **Results from constant volume *ab initio* calculations A-C**, Density of fractional shifts with temperature at constant volumes using the s-TDEP method from the two low energy transverse branch modes and for all modes (**D-F**). The mean(dashed color line), median (solid color line), and the 5^{th} and 95^{th} percentile (black solid lines) of the density are also shown. Calculations shown for (**A,D,G**) 99 % of 0 K volume, (**B,H,G**) 0 K volume, and (**C,F,I**) 101 % of 0 K volume. Quasiharmonic predictions are the dashed 0 lines in **A-F**. **G-I**, Corresponding constant volume differences between the quasiharmonic (QH) and s-TDEP in free energies from vibrational entropy with temperature.

Additional s-TDEP calculations of densities of thermal shifts suggest why the quasiharmonic theory has been so apparently successful. Calculations were performed for volumes that were 1% larger and 1% smaller than the 0 K harmonic volume calculated for Fig. 2.**A**, and the results are shown on the left and right sides of Fig. 3 for the TA modes (top three panels) and all phonon modes (middle three panels). For all three volumes, at low temperatures, there is a wide spread in the thermal phonon shifts, both stiffening and softening. At low temperatures, the average thermal shift from anharmonicity at a fixed volume is surprisingly nearly zero. At fixed volume, the shifts of all quasiharmonic phonons are zero, of course, so the two methods agree on the average owing to the cancellation of anharmonic stiffenings and softenings. This approximate cancellation is

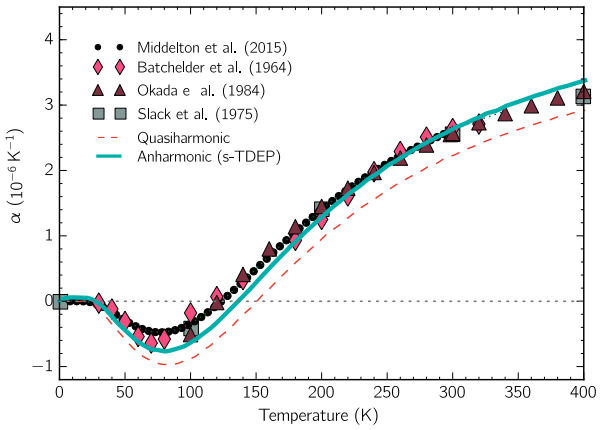

FIG. 4. **Calculated and experimental coefficients of linear thermal expansion in silicon.** Calculated coefficients are from minimized free energies using Supplementary Eq. 1 (s-TDEP: teal solid line, quasiharmonic (QH): red dashed line). Experimental values are shown as colored markers [7–10].

seen in Fig. 3.**A-C** for the TA modes and in Fig. 3.**D-F** for the all modes. Nevertheless, the average phonon energies from the s-TDEP method show an ordinary softening with increased volume and temperature, inconsistent with the negative Grüneisen parameters from quasiharmonic calculations. At high temperatures, Fig. 3.**D-F** show that all the modes tend to soften at similar rates. Differences in vibrational entropies from the s-TDEP and quasiharmonic methods were calculated using equations in the Supplementary Materials. The difference in entropies ΔS from the quasiharmonic and anharmonic was used to obtain the $-T\Delta S$ shown in Fig. 3.**G-I**. For all volumes, the differences are negligible up to 125 K but increase at higher temperatures (Fig. 4).

An independent concern about the quasiharmonic model is the elastic energies of thermal expansion, $\Delta E_{\text{el}} = 1/2Bv(\beta T)^2$, where B is the bulk modulus, β is the volume coefficient of thermal expansion, and v is the atomic volume. This ΔE_{el} should be comparable to the $-T\Delta S_{\text{vib}}$ contribution to the free energy from phonons. The maximum negative linear expansion at atmospheric pressure is 0.003 %, and the maximum positive linear expansion is 0.5% near the melting temperature [7, 8, 10]. The corresponding elastic energy for the negative thermal expansion is in the μeV range, and the positive thermal expansion gives approximately 0.2 meV at 500 K [7, 8, 10, 31]. These quasiharmonic energies are orders of magnitude smaller than the entropic contributions to the free energy.

We showed that a quasiharmonic model with negative Grüneisen parameters is physically incorrect, although some of its predictions of average properties are preserved by gross cancellations of errors. However, the success of the quasiharmonic theory implies that the diamond cubic structure is intrinsically prone to anomalies in thermal expansion. At low temperatures, the low energy transverse modes are more populated with phonons, so they must contribute to the decreased lattice parameter [4, 6]. The zero-point energy proves important for thermal expansion in silicon [22, 23], where the (fractional) population of the higher energy phonons alters the self-energies of TA phonons at low temperatures. Without the zero-point energy, the anharmonic calculations predict significantly different thermal expansion at low temperatures (Supplementary Materials), giving fundamental conflicts with classical mechanical models based on the "open-ness" of the structure, classical springs, force constant ratios, and negative Grüneisen parameters. Nevertheless, these phenomena may contribute to the general behavior, and are discussed in more detail in the Supplementary Materials. In silicon, anharmonic phonons and quantum effects are essential to the anomalous thermal expansion. A simple model has not yet been provided, as there probably is none.

Measurements of the phonon dispersions of single crystal silicon from 100 to 1500 K showed thermal shifts that contradict the trends predicted by the widely accepted quasiharmonic model, even at low temperatures. Pure phonon anharmonicity, i.e., phonon-phonon interactions, dominate the phonons in silicon from low to high temperatures, altering the effective interatomic potential and causing both positive and negative shifts of phonon energies. Although a mechanism for the anomalous thermal expansion of silicon remains a challenge, a detailed simulation that accounts for pure phonon anharmonicity successfully has reproduced the anomalous thermal expansion and the thermal shifts of phonons in silicon.

ACKNOWLEDGMENTS

The authors thank F.H. Saadi, A. Swaminathan, I. Papusha, and Y. Ding for assisting in sample preparation and discussions. Research at Oak Ridge National Laboratory's SNS was sponsored by the Scientific User Facilities Division, BES, DOE. This work used resources from NERSC, a DOE Office of Science User Facility supported by the Office of Science of the U.S. Department of Energy under Contract No. DE-AC02-05CH11231. Support from the Swedish Research Council (VR) program 637-2013-7296 is also gratefully acknowledged. Supercomputer resources were provided by the Swedish National Infrastructure for Computing (SNIC). This work was supported by the DOE Office of Science, BES, under contract DE-FG02-03ER46055.

* Electronic Address: dskim@caltech.edu

[1] Fultz, B., "Vibrational thermodynamics of materials," Prog. Mater. Sci. **55**, 247–352 (2010).

[2] B Fultz, *Phase transitions in materials* (Cambridge Univ. Press, Cambridge, 2014).

[3] A. A. Maradudin and A. E. Fein, "Scattering of Neutrons by an Anharmonic Crystal," Phys. Rev. **128**, 2589–2608 (1962).

[4] S Wei, C Li, and M.Y. Chou, "Ab initio calculation of thermodynamic properties of silicon." Phys. Rev. B **50**, 14587–14590 (1994).

[5] Zi-Kui Liu, Yi Wang, and ShunLi Shang, "Thermal Expansion Anomaly Regulated by Entropy," Sci. Rep. **4**, 7043 (2014).

[6] C.H. Xu, C.Z. Wang, C.T. Chan, and K.M. Ho, "Theory of the thermal expansion of Si and diamond." Phys. Rev. B **43**, 5024–5027 (1991).

[7] Thomas Middelmann, Alexander Walkov, Guido Bartl, and René Schödel, "Thermal expansion coefficient of single-crystal silicon from 7 K to 293 K," Phys. Rev. B **92**, 174113–7 (2015).

[8] Yasumasa Okada and Yozo Tokumaru, "Precise determination of lattice parameter and thermal expansion coefficient of silicon between 300 and 1500 K," J. Appl. Phys. **56**, 314–8 (1984).

[9] Glen A Slack and S. F. Bartram, "Thermal expansion of some diamondlike crystals," J. Appl. Phys. **46**, 89 (1975).

[10] D. N. Batchelder and R. O. Simmons, "Lattice Constants and Thermal Expansivities of Silicon and of Calcium Fluoride between 6° and 322°K," J. Chem. Phys. **41**, 2324–7 (1964).

[11] J. S. Shah and M. E. Strauman, "Thermal expansion behavior of silicon at low temperatures," Solid state Commun. **10**, 159–162 (1972).

[12] Olle Hellman, Peter Steneteg, I. A. Abrikosov, and S Simak, "Temperature dependent effective potential method for accurate free energy calculations of solids," Phys. Rev. B **87**, 104111 (2013).

[13] Bernard A Weinstein and G. J. Piermarini, "Raman scattering and phonon dispersion in Si and GaP at very high pressure," Phys. Rev. B **12**, 1172–1186 (1975).

[14] G Nilsson and G Nelin, "Study of the Homology between Silicon and Germanium by Thermal-Neutron Spectrometry," Phys. Rev. B **6**, 3777–3786 (1972).

[15] Alberto Debernardi, Stefano Baroni, and Elisa Molinari, "Anharmonic Phonon Lifetimes in Semiconductors from Density-Functional Perturbation Theory," Phys. Rev. Lett. **75**, 1819–1822 (1995).

[16] S. Narasimhan and D. Vanderbilt, "Anharmonic self-energies of phonons in silicon." Phys. Rev. B **43**, 4541–4544 (1991).

[17] M Balkanski, R. F. Wallis, and E Haro, "Anharmonic effects in light scattering due to optical phonons in silicon," Phys. Rev. B **28**, 1928–1934 (1983).

[18] C. Z. Wang, C. T. Chan, and K. M. Ho, "Empirical tight-binding force model for molecular-dynamics simulation of Si." Phys. Rev. B **39**, 8586–8592 (1989).

[19] José Menéndez and Manuel Cardona, "Temperature dependence of the first-order Raman scattering by phonons in Si, Ge, and α-Sn: Anharmonic effects," Phys. Rev. B **29**, 2051–2059 (1984).

[20] Raphael Tsu and Jesus Gonzalez Hernandez, "Temperature dependence of silicon Raman lines," Appl. Phys. Lett. **41**, 1016–1018 (1982).

[21] D.S. Kim, H.L. Smith, J.L. Niedziela, C.W. Li, D.L. Abernathy, and B. Fultz, "Phonon anharmonicity in silicon from 100 to 1500 K," Phys. Rev. B **91**, 014307 (2015).

[22] Philip B Allen, "Anharmonic phonon quasiparticle theory of zero-point and thermal shifts in insulators: Heat capacity, bulk modulus, and thermal expansion," Phys. Rev. B **92**, 064106–10 (2015).

[23] C. P. Herrero and R Ramírez, "Path-integral simulation of solids," J. Phys.: Condens. Matter **26**, 233201–36 (2014).

[24] D.L. Abernathy, M.B. Stone, M.J. Loguillo, M.S. Lucas, O Delaire, X Tang, J.Y.Y. Lin, and B Fultz, "Design and operation of the wide angular-range chopper spectrometer ARCS at the Spallation Neutron Source," Rev. Sci. Instrum. **83**, 015114 (2012).

[25] G.L. Squires, *Introduction to the Theory of Thermal Neutron Scattering* (Cambridge Univ. Press, Cambridge, 2012).

[26] H.R. Glyde, "Interference Effects in Neutron and X Ray Scattering," Can. J. Phys. (1974).

[27] B. N. Brockhouse, "Lattice Vibrations in Silicon and Germanium," Phys. Rev. Lett. **2**, 256–258 (1959).

[28] Jiao Y.Y. Lin, Hillary L. Smith, Garrett E Granroth, Douglas L Abernathy, Mark D Lumsden, Barry Winn, Adam A Aczel, Michael Aivazis, and Brent Fultz, "MCViNE - An object oriented Monte Carlo neutron ray tracing simulation package," Nucl. Instrum. Meth. A **810**, 86–99 (2016).

[29] Olle Hellman and I. A. Abrikosov, "Temperature-dependent effective third-order interatomic force constants from first principles," Phys. Rev. B **88** (2013).

[30] Ion Errea, Matteo Calandra, and Francesco Mauri, "Anharmonic free energies and phonon dispersions from the stochastic self-consistent harmonic approximation: Application to platinum and palladium hydrides," Phys. Rev. B **89**, 064302–16 (2014).

[31] S. P. Nikanorov, Yu A Burenkov, and A. V. Stepanov, "Elastic properties of si," Sov. Phys. Solid State **13**, 2516–2518 (1972).

[32] M B Stone, J L Niedziela, M J Loguillo, M A Overbay, and D L Abernathy, "A radial collimator for a time-of-flight neutron spectrometer," Review of Scientific Instruments **85**, 085101 (2014).

[33] "Mantid (2013): Manipulation and analysis toolkit for instrument data.; mantid project," (2013).

[34] O Arnold, J C Bilheux, J M Borreguero, A Buts, S I Campbell, L Chapon, M Doucet, N Draper, R Ferraz Leal, M A Gigg, V E Lynch, A Markvardsen, D J Mikkelson, R L Mikkelson, R Miller, K Palmen, P Parker, G Passos, T G Perring, P F Peterson, S Ren, M A Reuter, A T Savici, J W Taylor, R J Taylor, R Tolchenov, W Zhou, and J Zikovsky, "Mantid—Data analysis and visualization package for neutron scattering and μ SR experiments," Nucl. Instrum. Meth. A **764**, 156–166 (2014).

[35] S Doniach and M Sunjic, "Many-electron singularity in X-ray photoemission and X-ray line spectra from metals," Journal of Physics C: Solid State Physics **3**, 285–291 (1970).
[36] P E Blochl, "Projector augmented-wave method," Phys.Rev. **B50**, 17953–17979 (1994).
[37] G Kresse and J Furthmüller, "Efficiency of ab-initio total energy calculations for metals and semiconductors using a plane-wave basis set," Comoput. Mater. Sci. **6**, 15–50 (1996).
[38] G Kresse and J Hafner, "Ab initio molecular dynamics for liquid metals," Phys. Rev. B **47**, 558–561 (1993).
[39] G Kresse and J Hafner, "Ab initio molecular-dynamics simulation of the liquid-metal-amorphous-semiconductor transition in germanium," Phys. Rev. B **49**, 82513–14269 (1994).
[40] X Gonze and C Lee, "Dynamical matrices, born effective charges, dielectric permittivity tensors, and interatomic force constants from density-functional perturbation theory," Phys. Rev. B **55**, 10355–10368 (1997).
[41] R Armiento and A E Mattsson, "Functional designed to include surface effects in self-consistent density functional theory," Phys. Rev. B **72**, 085108–5 (2005).
[42] Ann E Mattsson and Rickard Armiento, "Implementing and testing the AM05 spin density functional," Phys. Rev. B **79**, 155101–13 (2009).
[43] Ann E Mattsson, Rickard Armiento, Joachim Paier, Georg Kresse, John M Wills, and Thomas R Mattsson, "The AM05 density functional applied to solids," The Journal of Chemical Physics **128**, 084714–12 (2008).
[44] Duane C Wallace, *Thermodynamics of Crystals* (Wiley, New York, 1972).
[45] Martin T Dove, *Introduction to Lattice Dynamics* (Cambridge University Press, 1993).
[46] J. L. Feldman, L. L. Boyer, P. J. Edwardson, and J. R. Hardy, "Calculation of Dielectric Susceptibility for Complex Ionic Systems - Application to a Predicted Superlattice," Phys. Rev. B **40**, 4105–4118 (1989).

SUPPLEMENTARY MATERIALS

Materials and Methods

Inelastic Neutron Scattering

Inelastic neutron scattering measurements were performed on a single crystal of silicon of 99.999% purity that was highly-oriented ($< 2^\circ$), purchased from Virginia Semiconductor, Inc. The [110] oriented single crystal was further machined into a cylinder of 3.8 cm in height, 2.54 cm in outer diameter and a 1.59 cm inner diameter to minimize multiple scattering. The crystal was suspended in an aluminum holder and then mounted into a closed-cycle helium refrigerator for the 100 and 200 K measurements, and a similar holder made from niobium was mounted into a low-background electrical resistance vacuum furnace for measurements at 300, 900, 1200 and 1500 K. For all measurements the incident energy was 97.5 meV, and an oscillating radial collimator was used to reduce background and multiple scattering [24, 32].

The time-of-flight neutron data included multiple datasets from 200 rotations in increments of 0.5° about the vertical [110]-axis, reduced to create the full $S(\mathbf{q},\varepsilon)$ using standard software [33, 34]. A secondary data reduction process consisted of 'folding' the entire $S(\mathbf{q},\varepsilon)$ data set into an irreducible wedge in the first Brillouin zone. Non-linear offsets of the $\mathbf{q}$-grid were corrected by fitting typically 50 *in situ* Bragg diffractions in an energy transfer range of $\Delta\varepsilon = \pm 4$ meV by a transformation to the positions of the theoretical diffraction peaks for a diamond cubic structure. The corrected grid was then 'folded back' and corrected for the phonon creation thermal factor [25]. The correct alignment of the reciprocal space dataset produced $S(\mathbf{q},\varepsilon)$ of high statistical quality.

Energy spectra at specific $\mathbf{q}$-points mentioned were evaluated by integrating over 0.0025 Å^{-3}. Phonon centroids were then fitted using the Levenberg-Marquardt non-linear least square method for multiple Doniach model functions [35]. Examples of the scattered intensities at a constant-$\mathbf{q}$, with fits, are shown for the X-point in Fig. S1.

Ab-initio Calculations

Ab initio DFT calculations were performed with the projector augmented wave [36] formalism as implemented in VASP [37–40]. All calculations used a $5 \times 5 \times 5$ supercell and a 500 eV plane wave energy cutoff. The Brillouin zone integrations used a $3 \times 3 \times 3$ k-point grid, and the exchange-correlation energy was calculated with the AM05 functional [41–43].

Finite temperature phonon dispersions of silicon were calculated by fitting first-principles forces to a model hamiltonian,

$$H = U_0 + \sum_i \frac{\mathbf{p}_i^2}{2m} + \frac{1}{2}\sum_{ij\alpha\beta} \Phi_{ij}^{\alpha\beta} u_i^\alpha u_j^\beta + \frac{1}{3!}\sum_{ijk\alpha\beta\gamma} \Phi_{ijk}^{\alpha\beta\gamma} u_i^\alpha u_j^\beta u_k^\gamma. \quad (1)$$

The forces on atoms were generated using DFT through various configurations of displaced atoms by a stochastic sampling of a canonical ensemble, with cartesian displacements (u_i^α) normally distributed around the mean thermal displacement using

$$u_i^\alpha = \sum_k \frac{\epsilon_k^{i\alpha} c_k}{\sqrt{m_i}} \sqrt{-2\ln\xi_1}\sin(2\pi\xi_2). \quad (2)$$

The thermal factor, c_k, is based on thermal amplitudes of normal mode k, with eigenvector ϵ_k and frequency ω_k

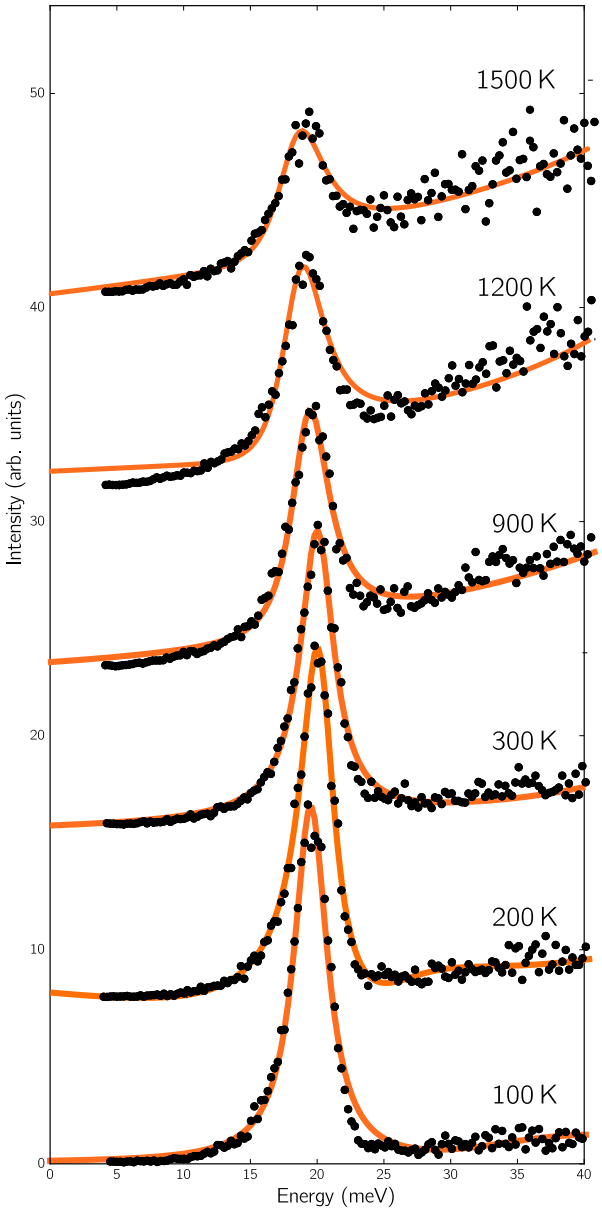

FIG. 5. Constant $\mathbf{q}$-S($\mathbf{q}$,ε) data at the X point for 100, 200, 300, 900, 1200, 1500 K. Data are black markers and fits are in orange.

[30, 44, 45]

$$c_k = \sqrt{\frac{\hbar(2n_k+1)}{2\omega_k}}, \tag{3}$$

and ξ_1 and ξ_2 are stochastically sampled numbers between 0 and 1.

The fitting to the model Hamiltonian used the temperature-dependent effective potential method (TDEP) [12, 29]. With thermal displacements from Eq S2 and Eq. S3, we refer to our temperature-dependent calculations as the stochastically-initialized temperature-dependent effective potential method (s-TDEP). This method circumvents the issue of expensive computational resources required of *ab initio* molecular-dynamics (AIMD), replacing AIMD with a Monte Carlo sampling of atomic positions and momentum near equilibrium positions [12, 30]. The quasiharmonic model was calculated as described previously [21].

Thermodynamic Calculations

Temperature dependent coefficients of linear thermal expansion in silicon were calculated through the minimization of the free energy,

$$F(T,V) = E(T,V) + \sum_{\mathbf{q},k}\Big(\frac{\hbar\omega_k(\mathbf{q},V,T)}{2} + k_\mathrm{B}T\ln(1-e^{-\hbar\omega_k(\mathbf{q},T,V)/k_\mathrm{B}T})\Big), \tag{4}$$

from quasiharmonic calculations, and from s-TDEP (main text Fig. 5). The quasiharmonic model implies the only temperature dependence of the entropy is from the volume expansion ($\varepsilon_i(V\{T\})$) and the Planck distribution (n_k) whereas the anharmonic s-TDEP method minimizes the free energy for temperature and volume simultaneously. The vibrational entropy from all phonon modes, $\sum_k$, was calculated as [1],

$$S_\mathrm{vib}(T) = 3k_\mathrm{B}\sum_k\big[(n_k+1)\ln(n_k+1) - n_k\ln(n_k)\big]. \tag{5}$$

Possible Contributions to the Thermal Expansion

As stated in the main text, a simple physical model for the anomalous thermal expansion of silicon is unlikely because different effects contribute to the thermal expansion. In particular, the anharmonicity and nuclear quantum effects are difficult to formulate as a simple 3D model. The thermal expansion of Si can be simulated properly with methods based on *ab initio* calculations that includes all these factors, but this seems unsatisfying for a "physical" understanding. A number of possible contributions and models are presented here, but any single model is insufficient by itself.

Negative Grüneisen Parameters as Fitting Parameters

If individual Grüneisen parameters are assigned to different parts of the phonon DOS, it is easy to make a model that predicts negative thermal expansion at low temperatures. An approximation for silicon is shown in Fig. 6,

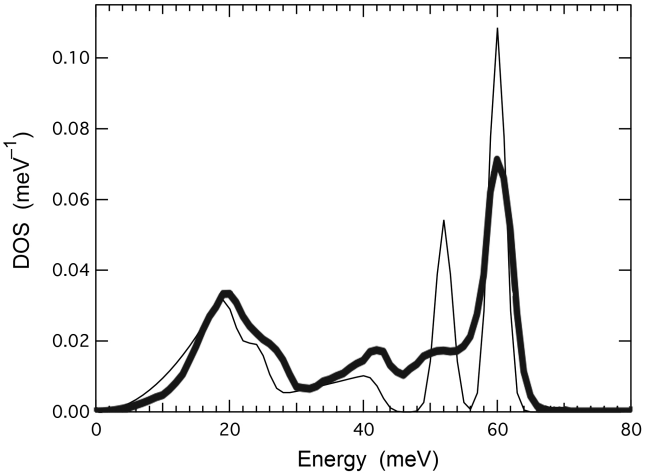

FIG. 6. Phonon DOS of Si from (thick line) experimental measurement at 100 K [21], and (thin line) approximated with Debye and Einstein models.

together with the experimental phonon DOS reported previously [21]. The six phonon branches were modeled as follows: acoustic branches were approximated by Debye models with cutoff energies of 20, 25, 42 meV, and optical branches were approximated as Einstein modes with energies of 52, 60, 60 meV. These curves were convoluted with a Gaussian function of standard deviation $\sqrt{3}$ meV, summed, and are compared to the experimental phonon DOS of Si [21] in Fig. 6.

The heat capacities of these six functions were calculated as shown in Fig. 7.a. For simplicity, a Grüneisen parameter of −1 was assigned to the lowest-energy TA modes, and a Grüneisen parameter of +1 was assigned to the other five phonon branches. The thermal expansion as a function of temperature, shown in Fig. 7.b, has a shape that follows the heat capacity curves times their Grüneisen parameters. At low temperatures, the negative contribution from the TA1 modes overcomes the positive contribution from the TA2 modes, but the thermal expansion changes sign when the LA modes are sufficiently occupied. With six Grüneisen parameters, there are many ways to optimize the thermal expansion as a function of temperature, and the depth and breadth of the minimum can be tuned by appropriate parameter selection. We did not explore this further because the main text shows that this approach is physically incorrect.

Simple Springs and Angular Bonds

The simplest model of harmonic interatomic forces is useful for illustrating a geometrical source of phonon anharmonicity. Fig. 8.a shows a tetrahedron with a Si atom surrounded by its nearest neighbors. The four bonds are

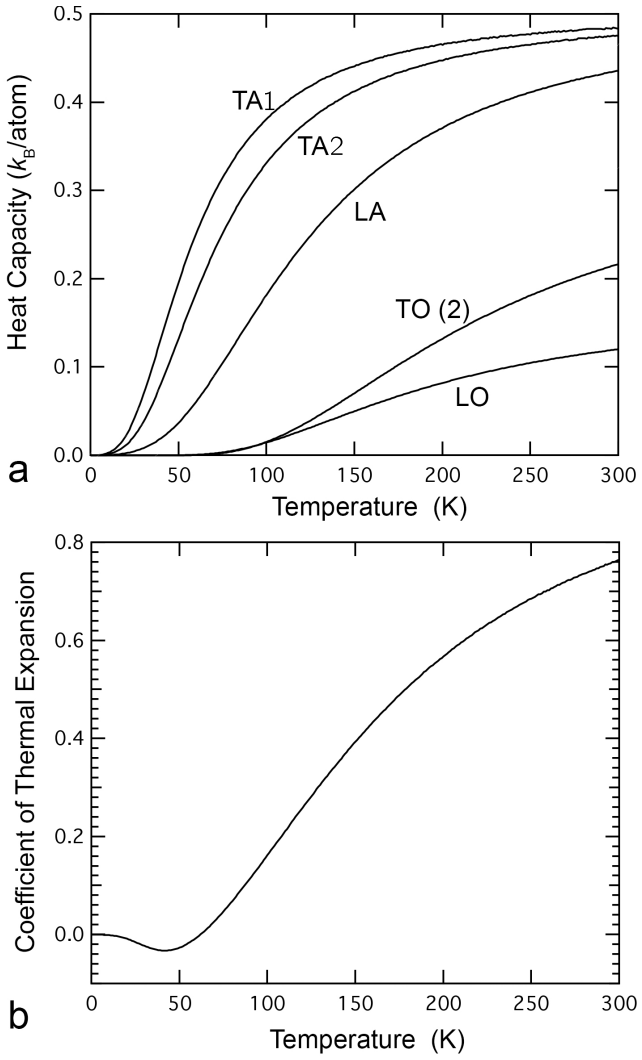

FIG. 7. (**a**) Heat capacities from phonons approximated by Debye and Einstein models, using the six branches of Fig. 6. (**b**) Coefficient of thermal expansion, assuming all Grüneisen parameters were +1 except for TA modes set as –1.

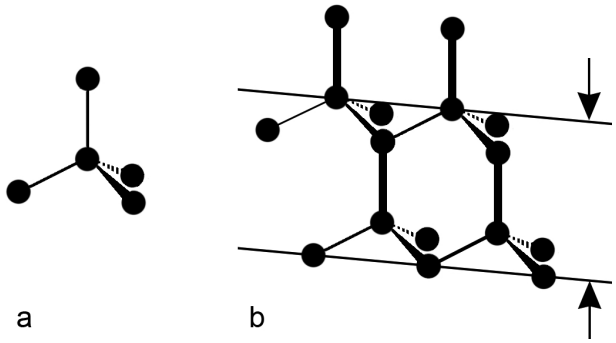

FIG. 8. **a**, Tetrahedral coordination around a central Si atom. **b**, four interconnected tetrahedra of the diamond cubic structure. Thick vertical lines are along a [111] direction.

assumed to be harmonic springs, and it can be initially assumed that the neighbors remain fixed in position. As shown in Fig. 8.a, the springs are relaxed, with no elastic energy. If the central Si atom is displaced vertically, the amount of elastic energy stored in the spring to the neighbor above is the same for positive and negative displacements of equal magnitude. This symmetry does not hold for the lower three springs. Upwards displacements are more along the directions of the springs, and generate more elastic energy than downwards displacements. The elastic energy is straightforward to calculate for harmonic springs in a tetrahedral coordination with angles of 109.5° and a nearest-neighbor separation of a. For vertical displacements, x, a numerical fit to the elastic energy in all four springs gives

$$E_{\mathrm{el}}(x) \propto \left(\frac{x}{a}\right)^2 + 0.666\left(\frac{x}{a}\right)^3 , \qquad (6)$$

so negative x (downwards) displacements are more favorable energetically. The lengthening of the vertical bond in Fig. 8.a gives positive thermal expansion, and it is likely important at high temperatures when numerous short wavelength phonons disrupt the cooperative displacements between adjacent tetrahedra.

For long wavelength phonons, however, displacements along the [111] direction can provide for negative thermal expansion. Fig. 8.b helps to illustrate a phonon mode where the vertical Si pairs along [111] maintain a fixed separation, and vibrate as a unit along the [111] direction. For the case shown in Fig. 8.b, the cubic anharmonicity of Eq. S6 will cause a decrease in separations between planes of atoms, illustrated by the arrows. For a 1% mean-squared displacement, Eq. S6 predicts that the cubic term is approximately 1% of the magnitude of the quadratic. We might expect the lattice parameter to decrease by approximately one part in 10^{-4} if such modes dominate. The complexity of accounting for all different modes and their thermal occupancies makes further analysis impractical, however. These examples show

- When atom displacements are not along the directions of the springs, phonon modes can be anharmonic even when the springs are harmonic.

- These geometrically-induced anharmonicites can change sign with the wavevector of the phonon mode.

The influence of anharmonicity may also be expected because the geometrical structure of silicon does not have inversion symmetry at each atom. This allows cubic phonon-phonon interactions in first order [3, 46], making vibrational modes more free to exchange energy.

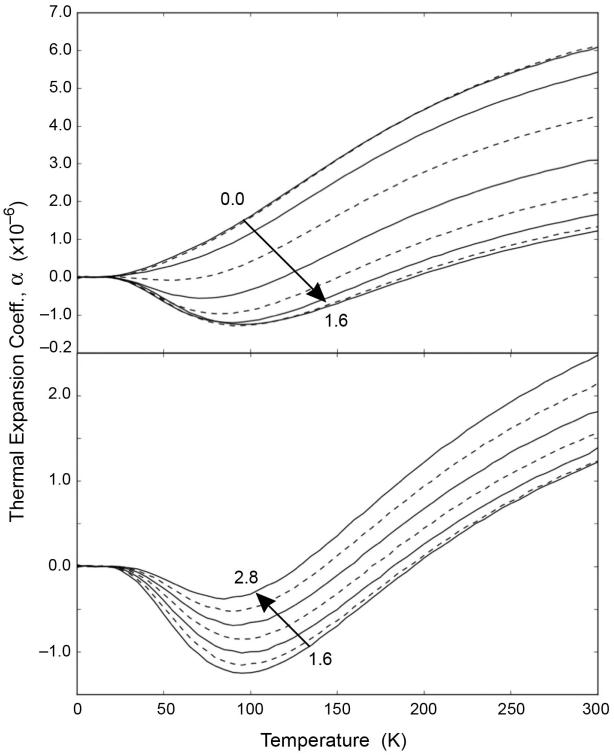

FIG. 9. Trends for silicons thermal expansion coefficient vs. temperature plotted for scalings of the ratio of transverse to longitudinal force constants between 0 and 2.8

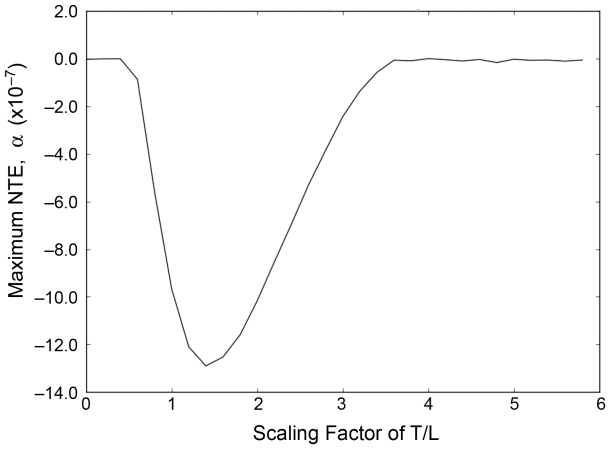

FIG. 10. Maximum negative thermal expansion coefficients taken from each trend in Figure S5 plotted against the scaling factor, k, applied to the ratios of transverse to longitudinal force constants.

Transverse Bonds

The diamond cubic structure is not stable under longitudinal forces alone, and transverse forces are required to prevent its collapse into a denser structure. Xu, et al., argue that the negative thermal expansion of silicon depends on

the relative strengths of the first-nearest-neighbor bond-bending and bond-stretching forces [6]. For two specific phonon modes (TA($\mathbf{q}$=X) and TA($\mathbf{q}$=L)), they develop a mechanical model that predicts negative Grüneisen parameters when both central forces and non-central forces are of comparable strength. They note that the relative strength of the non-central forces plays a major role in setting the thermal expansion of silicon [6].

We decomposed pairwise interactions between silicon atoms, quantified as force constant tensors into components that are transverse and longitudinal to the relevant bond. Interestingly, we found that with a model quasiharmonic system that there is some optimal scaling of the transverse to longitudinal force constants that results in maximal negative thermal expansion in Si. (Although the simple modes described previously in Section B have no transverse forces but have negative Grüneisen parameters, there are many other modes that contribute to the thermal expansion.)

To do this, we began with force constant tensors that describe pairwise interactions between the atom at each of the two distinct symmetry positions in silicon and its closest 123 neighbors as a function of volume at 0 K. For each pairwise interaction between each of the atoms at distinct symmetry positions and its neighbors, we decomposed the force constant tensor into components transverse and longitudinal to the bond between the pair of atoms. We scaled the ratio of transverse to longitudinal force constants by a constant, k, while holding fixed the norm of the force constant tensor. We then calculated the the thermal expansion in silicon for values of k between 0 and 2.8. In Fig. 9, we show that increasing the ratios of transverse to longitudinal force constants in the system for values of k between 0 and about 1.6 increases the amount of negative thermal expansion, and that increasing k beyond 1.6 decreases negative thermal expansion. In Fig. 10, we illustrate the dependence of the negative thermal expansion on the ratios of transverse to longitudinal force constants by plotting the minimum value of thermal expansion exhibited by the system (one metric for quantifying the degree of NTE) against the scaling constant k. Although the quasiharmonic approximation should not be used to predict how negative Grüneisen parameters give the negative thermal expansion of silicon, the ratio of forces should influence on the thermal expansion of diamond cubic structures.

Quantum and Zero-point Effects

The models in transverse bonds, and simple springs sections, like many other previous models, can be understood with classical mechanics. This is know to be inadequate [22, 23]. Using Eq. S5 for classical or quantum distributions in Eq. S4 for the free energy give major differences in thermal expansion in silicon, as shown in Fig. 11. Even at lower temperatures, the zero-point energy brings importance to all the phonon modes. Not only are quantum effects essential at lower temperatures, but differences persist up to melting temperatures.

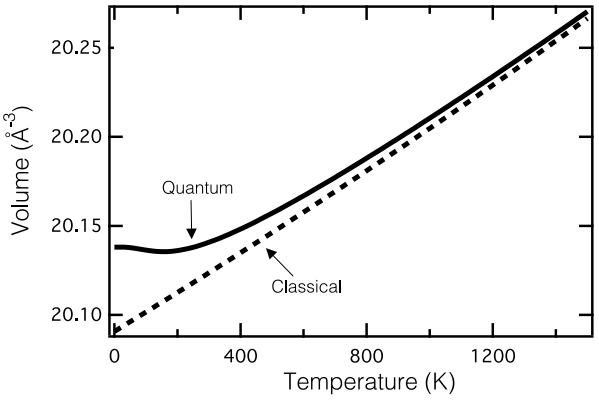

FIG. 11. Volume vs. temperature for silicon obtained from classical and quantum mechanical free energies.

In general, all of the models explained above are effective for a pedagogical thought exercise for a "physical interpretation" of the negative thermal expansion of silicon, but no single simple model is able to capture the full behavior.